A Model of Volumetric Shape for the Analysis of Longitudinal Alzheimer's Disease Data*

Xinyang Liu[1], Xiuwen Liu[2], Yonggang Shi[3], Paul Thompson[3], and Washington Mio[1]

[1] Department of Mathematics, Florida State University, Tallahasse, FL 32306
[2] Department of Computer Science, Florida State University, Tallahasse, FL 32306
[3] Laboratory of NeuroImaging, UCLA School of Medicine, Los Angeles, CA 90095

Abstract. We develop a multi-scale model of shape based on a volumetric representation of solids in 3D space. A signed energy function (SEF) derived from the model is designed to quantify the magnitude of regional shape changes that correlate well with local shrinkage and expansion. The methodology is applied to the analysis of longitudinal morphological data representing hippocampal volumes extracted from one-year repeat magnetic resonance scans of the brain of 381 subjects collected by the Alzheimer's Disease Neuroimaging Initiative. We first establish a strong correlation between the SEFs and hippocampal volume loss over a one-year period and then use SEFs to characterize specific regions where hippocampal atrophy over the one-year period differ significantly among groups of normal controls and subjects with mild cognitive impairment and Alzheimer's disease.

Keywords: Shape space, volumetric shape, hippocampal atrophy, Alzheimer's disease, ADNI.

1 Introduction

We construct shape spaces and metrics that provide a framework for the analysis of volumetric morphological data. We use the model to quantify and compare regional and global shape changes in the hippocampus (HC) due to normal aging, tissue loss caused by conversion to Alzheimer's disease (AD) and progression of the disorder over a one-year period.

AD is the most common form of dementia and afflicted more than 26 million elderly individuals worldwide in 2006; it is projected that, globally, an average of 1 in 85 people will suffer from the disorder by 2050. AD is a neurodegenerative disease and patients experience severe memory loss and progressive decline of various cognitive functions. Studies that track the propagation of neurodegeneration in AD (cf. [1,2]) indicate that the medial temporal lobe structures, including the hippocampus, are among the first to degenerate. As such, the hippocampus

* This research was supported in part by NSF grants DMS-0713012 and CCF-0514743, and NIH Roadmap for Medical Research grant U54 RR021813.

K. Daniilidis, P. Maragos, N. Paragios (Eds.): ECCV 2010, Part III, LNCS 6313, pp. 594–606, 2010.

has been the focus of many studies of AD, which demonstrate considerable volume loss in the left and right hippocampi as the disease progresses (cf. [3,4] and references therein). Changes in hippocampal shape in AD have also been modeled with large deformation diffeomorphisms (cf. [5]). Although presently there is no cure, mapping the patterns of propagation of tissue loss and advances in early diagnosis will potentially enhance clinical trials that increase our understanding of the disorder and also help in the management of the disease, as symptomatic therapy is likely to be more effective before severe neurodegeneration occurs.

The Alzheimer's Disease Neuroimaging Initiative (ADNI) is a major multisite study of AD to determine whether brain imaging can help to predict onset and monitor the progression of AD [6,7]. ADNI is a longitudinal MRI (magnetic resonance imaging) and FDG-PET (fluorodeoxyglucose positron emission tomography) study of 800 elderly subjects. One of the main goal of ADNI is data collection for subsequent analysis; existing studies of the hippocampus based on ADNI data include [4,8,9]. The morphological analysis of the hippocampus carried out in this paper employs a subset of the ADNI dataset comprising two scans of each of 381 subjects acquired one year apart. At each scan acquisition, an individual is classified as normal (NL), with mild cognitive impairment (MCI), or with AD. This classification naturally divides the subjects into four groups: NL-NL, MCI-MCI, MCI-AD and AD-AD. Table 1 shows the breakdown of the 381 individuals included in this study for a total of 762 scans. MCI may be viewed as a transitional stage to dementia, even though conversion may not necessarily occur. MCI patients are of particular interest because they exhibit an increased risk of conversion and the MCI-AD group represent the early stages of the disease.

Table 1. Subset of 381 ADNI subjects used in this study

Group	# of Subjects	Group	# of Subjects
NL-NL	118	MCI-MCI	153
MCI-AD	39	AD-AD	71

In this paper, we present a shape model equipped with a multi-scale Sobolev-type metric to quantify volumetric similarity and divergence of solids in 3D Euclidean space. We develop volumetric models of shape because they are potentially more sensitive to morphological changes caused by neurodegeneration than models just based on contour surfaces. The model may be viewed as a continuous extension of classical Procrustes analysis of shapes [10] to solids in 3D space. One major difference, however, is that the metric employed is base not only on the relative positions of points, but also on the first derivatives of parametrizations. First-order metrics are more sensitive to local non-linear deformations such as local contractions or expansions. To suppress the undesirable effect of very small variations or noise, the first-order term is smoothed out with the Riemannian heat operator (cf. [11]). This model provides a framework for the development of a tool, which we refer to as the signed energy function (SEF),

to quantify localized shape contrasts in populations. We show that measures derived from SEF correlate well with volume loss in the hippocampus, an important indicator that SEF is sensitive to the morphology of neurodegeneration.

For each subject, the hippocampal volume was segmented from the whole-brain MRI scan using the techniques of [4]. First, triangular meshes were constructed to represent the contour surfaces of all hippocampi. Following a standard procedure, one of the NL meshes was fixed as a reference and all other surfaces were registered with it with the direct mapping method of [12]. Then, the registration of the surfaces was extended to hippocampal volumes using a thin-plate-spline interpolant [13]. For computations, the registered left hippocampal volumes were discretized as "cubical" meshes with 3,908 vertices and 10,533 edges, while the right hippocampus was represented with 3,796 vertices and 10,219 edges. For each subject, the SEF was calculated between the baseline and follow-up scans. For each group, we applied the SEFs to the localization of specific regions with statistically significant shape differences linked with local shrinkage. Moreover, we compared the left hippocampus of the AD-AD group with all other groups, as well as the right hippocampus of the MCI-AD group with the others, since these two groups showed more significant shape changes.

The paper is organized as follows. In Section 2 we present the continuous model of volumetric shape. The signed energy function is discussed in Section 3 and the discretization of the model is sketched in Section 4. Applications of the model to Alzheimer's disease are presented in Section 5.

2 A Multi-scale Model of Shape

2.1 Sobolev Metrics

Let V be a connected solid in 3D space with a smooth contour surface. V will be fixed throughout as a reference domain. A parametric shape will be represented by a mapping $\alpha\colon V \to \mathbb{R}^3$, with coordinates $\alpha(p) = [\,\alpha_1(p)\ \alpha_2(p)\ \alpha_3(p)\,]^T$. We impose Neumann boundary conditions $\nabla\alpha_i(p) \cdot \nu(p) = 0$, for every p on the boundary ∂V, where $\nu(p)$ is the outer unit normal at $p \in \partial V$. If we denote the differential of α at p by $d\alpha_p\colon \mathbb{R}^3 \to \mathbb{R}^3$, the usual first-order Sobolev metric on V may be expressed as

$$\langle \alpha, \beta \rangle = \int_V \alpha(p) \cdot \beta(p)\, dp + \int_V \langle d\alpha_p, d\beta_p \rangle\ dp\,, \tag{1}$$

where $\langle d\alpha_p, d\beta_p \rangle = \mathrm{tr}\,(d\alpha_p \circ d\beta_p^*)$ and $d\beta_p^*$ is the adjoint of $d\beta_p$. This coincides with the usual Euclidean inner product of matrices under the matrix representation of differentials relative to an orthonormal basis.

Since the first-order term can be very sensitive to small deformations and noise, we modify the metric by smoothing it out via the heat kernel. Smoothing of the first-order term also leads to more stable computations. Let $0 = \lambda_0 < \lambda_1 \le \lambda_2 \le \cdots \uparrow \infty$ be the eigenvalues of the Laplacian on V subject to Neumann

boundary conditions. We denote an associated orthonormal set of eigenfunctions by ϕ_i, $i \geqslant 0$. The heat kernel on V may be expressed as

$$K(p,q,t) = \sum_{i=0}^{\infty} e^{-\lambda_i t} \phi_i(p) \phi_i(q)\,. \tag{2}$$

For each fixed $t > 0$, we obtain a smoothed out version of α via the kernel K given by $\alpha^t(p) = [\,\alpha_1(p;t)\ \alpha_2(p;t)\ \alpha_3(p;t)\,]^T$, where

$$\alpha_i(p;t) = \int_V K(p,q,t)\alpha_i(q)\,dq\,. \tag{3}$$

The Sobolev metric (1) is modified to

$$\langle \alpha, \beta \rangle_t = a \int_V \alpha(p) \cdot \beta(p)\,dp + b \int_V \left\langle d\alpha_p^t, d\beta_p^t \right\rangle\,dp\,. \tag{4}$$

We also introduce weights $a, b > 0$ to be able to adjust the contributions of the two terms, as desired, and normalize them to satisfy $a + b = 1$. Note that the smoothing operator is only applied to the derivative term. The associated norm is denoted $\|\cdot\|_t$.

2.2 The Shape Model

As in conventional Procrustes analysis, to obtain a representation of shape that is invariant under translations, we place the centroid of α at 0 by requiring that $\int_V \alpha_i(p)\,dp = 0$, for $1 \leqslant i \leqslant 3$. As in Kendall's formulation [10] and the surface model of [14], we could also normalize size with respect to the proposed metric. However, we shall skip this step since one of our main goals is to use the metric to detect change in shape and size caused by atrophy. Thus, the proposed model is sensitive to scale. We also need to enforce invariance under change of orientation via the action of the group $O(3)$ of 3×3 orthogonal matrices. If $U \in O(3)$, the action of U on α is given by $\alpha \mapsto U\alpha$. Clearly, this is an action by isometries, i.e., $\langle U \circ \alpha, U \circ \beta \rangle_t = \langle \alpha, \beta \rangle_t$. Moreover, if U, $W \in O(3)$,

$$\langle W \circ \alpha, U \circ \beta \rangle_t = \left\langle \alpha, W^T U \beta \right\rangle_t = \left\langle \alpha, \widetilde{U}\beta \right\rangle_t\,, \tag{5}$$

where $\widetilde{U} = W^T U$. Thus, to calculate the shape distance, one may fix α and only apply orthogonal transformations to β. If s_α, s_β are the shapes represented by α and β, the shape distance is defined as

$$d_t(s_\alpha, s_\beta) = \min_{U \in O(3)} \|\alpha - U \circ \beta\|_t = \|\alpha - \widehat{U} \circ \beta\|_t\,, \tag{6}$$

where $\widehat{U}$ is the orthogonal transformation that minimizes the distance. To find $\widehat{U}$, we extend the classical Procrustes alignment of configurations of landmarks

to the present setting. Let $\alpha = [\alpha_1, \alpha_2, \alpha_3]^T$ and $\beta = [\beta_1, \beta_2, \beta_3]^T$. Consider the 3×3 matrix A, whose (i, j)-entry is

$$a_{ij} = \langle \alpha_i, \beta_j \rangle_t = a \int_V \alpha_i(p)\beta_j(p)\, dp + b \int_V \nabla\alpha_i(p;t) \cdot \nabla\beta_j(p;t)\, dp\,. \tag{7}$$

If $A = V_1 \Sigma V_2^T$ is an singular value decomposition of A, one can show that $\widehat{U} = V_1 V_2^T$ [15].

3 Signed Energy Function

In practical applications of the model, we are interested not only in the shape metric as a global quantifier of shape dissimilarity, but also in localization tools to detect specific regions where shape divergence is most significant. To design such a tool notice that, although the shape distance (6) has a global nature, the total deformation energy (the square of the shape distance) is an integral of pointwise energies. More precisely, letting $\hat{\beta} = \widehat{U} \circ \beta$, (4) and (6) imply that

$$d_t^2(s_\alpha, s_\beta) = \int_V \left(a\|\alpha(p) - \hat{\beta}(p)\|^2 + b\|d\alpha_p^t - d\hat{\beta}_p^t\|_p^2 \right)\, dp\,. \tag{8}$$

Thus, we define the energy function $E_{\alpha,\beta}^t \colon V \to \mathbb{R}$ by

$$E_{\alpha,\beta}^t(p) = a\|\alpha(p) - \hat{\beta}(p)\|^2 + b\|d\alpha_p^t - d\hat{\beta}_p^t\|_p^2\,. \tag{9}$$

The local energy $E_{\alpha,\beta}^t(p)$ quantifies how much the shapes of α and β differ near p from the standpoint of the metric d_t. Note, however, that the energy associated with local shape changes due to local shrinkage and expansion are both non-negative. This raises the question of whether it is possible to modify $E_{\alpha,\beta}^t$ to a signed measurement that can better differentiate these two types of deformation. This is of particular interest in applications to neurodegenerative diseases such as AD. Here, we propose a simple approach to this problem and show in Section 5 that the modified energy function correlates well with total hippocampal volume loss. Assume that α and β are centered and orthogonally aligned. We attribute a '+' sign to $E_{\alpha,\beta}^t(p)$ if $\|\alpha(p)\| \geqslant \|\hat{\beta}(p)\|$ and a negative sign, otherwise. In other words, the sign is positive if the Euclidean distance to the centroid decreases as we change α to β and negative if it increases. Thus, a positive or negative signed energy function (SEF) should indicate local shrinkage or expansion, respectively.

4 The Discrete Model

We briefly sketch the discretization of the model of Section 2. We discretize the reference volume V in 3D space as a regular cubical mesh K with edge length ℓ. Let $\mathcal{V} = \{v_1, v_2, \cdots, v_n\}$ and $\mathcal{E} = \{e_1, e_2, \cdots, e_m\}$ be the vertex and edge sets of K, respectively. We fix an arbitrary orientation for each edge $e_i \in \mathcal{E}$. A discrete parametric shape α is represented by a piecewise linear map $K \to \mathbb{R}^3$, so that α

is completely determined by its values on the vertices of K. Therefore, α can be viewed as a $3 \times n$ matrix, where the jth column represents $\alpha(v_j) \in \mathbb{R}^3$.

We use the discrete exterior derivative to represent the differential of α, which is defined on $\mathcal{E}$. For the oriented edge $e_j \in \mathcal{E}$, we let $d\alpha(e_j) = \left[\alpha(e_j^+) - \alpha(e_j^-)\right]/\ell$, where e_j^+ and e_j^- are the terminal and initial vertices of e_j, respectively. Thus, the derivative can be viewed as a $3 \times m$ matrix, whose jth column represents $d\alpha(e_j) \in \mathbb{R}^3$. To discretize the inner product (4), we first discuss the discrete volume elements. For the first term, it is simply the volume ℓ^3 of the voxels of K. For the second, we use the volume "around" each edge e_j, which is calculated as follows. Each cube σ incident with e_j contributes $\ell^3/12$ to this volume. Thus, for an interior edge, the volume around e_j is $\ell^3/3$.

We use a standard finite-difference discretization of the Laplacian and the eigenvalues and eigenvectors are calculated using the Lanczos subspace method. In computations, we truncate the discrete version of (2) after the first $r+1$ eigenvalues based on experimental experience. Therefore, for a vertex v, the expression (3) becomes

$$\alpha_i(v;t) = \ell^3 \sum_{k=0}^{r} \sum_{j=1}^{n} e^{-\lambda_k t} \phi_k(v) \phi_k(v_j) \alpha_i(v_j)\,, \tag{10}$$

The Sobolev inner product (4) can now be discretized as

$$\langle \alpha, \beta \rangle_t = a\ell^3 \sum_{i=1}^{n} \alpha(v_i) \cdot \beta(v_i) + \frac{b\ell^3}{3} \sum_{j=1}^{m} d\alpha^t(e_j) \cdot d\beta^t(e_j). \tag{11}$$

Finally, the value of the energy function in (9) at a vertex v is

$$E^t_{\alpha,\beta}(v) = a\|\alpha(v) - \hat{\beta}(v)\|^2 + \frac{b}{6} \sum_j \|d\alpha^t(e_j) - d\hat{\beta}^t(e_j)\|^2\,, \tag{12}$$

where j varies over the indexes of the edges incident with v.

5 Experimental Results

As mentioned in the Introduction, after segmentation of the hippocampal volumes and registration of their contour surfaces, we extended the point correspondences to their entire volumes through a thin-plate-spline interpolant [13]. Using a subset of the baseline scans of normal controls, we construct a hippocampal atlas V as a sample mean shape. We adopted the Fréchet mean shape with respect to the shape metric proposed, that is, the minimizer of the sum of the square shape distances (cf. [8,14]). A regular cubical mesh K was then generated to represent the hippocampal atlas. The atlas reflects the anatomical characteristics shared by the members of a population and provides a common domain

for comparison and analysis of different individuals and groups. To obtain compatible meshes, we transferred the cubical mesh K of the atlas via the volume registration to all the other hippocampi. This gives a parametric representation of all shapes over K. We then calculated the shape distance between the baseline and 12-month hippocampal volumes of each subject and their associated SEF. The parameters were set to $a = 0.9$, $b = 0.1$, $t = 0.01$ and $r = 49$. These values were chosen experimentally.

As explained in Section 3, we expect the signed energy functions to reflect shape changes associated with local shrinkage and expansion effectively. Therefore, to make a more convincing case, we first show that our measure of volume loss is consistent with results obtained in other studies and verify that SEFs correlate well with volume loss during the one year period. We then proceed to a finer analysis to detect specific regions where the shape changes in the NL-NL, MCI-MCI, MCI-AD and AD-AD groups differ significantly.

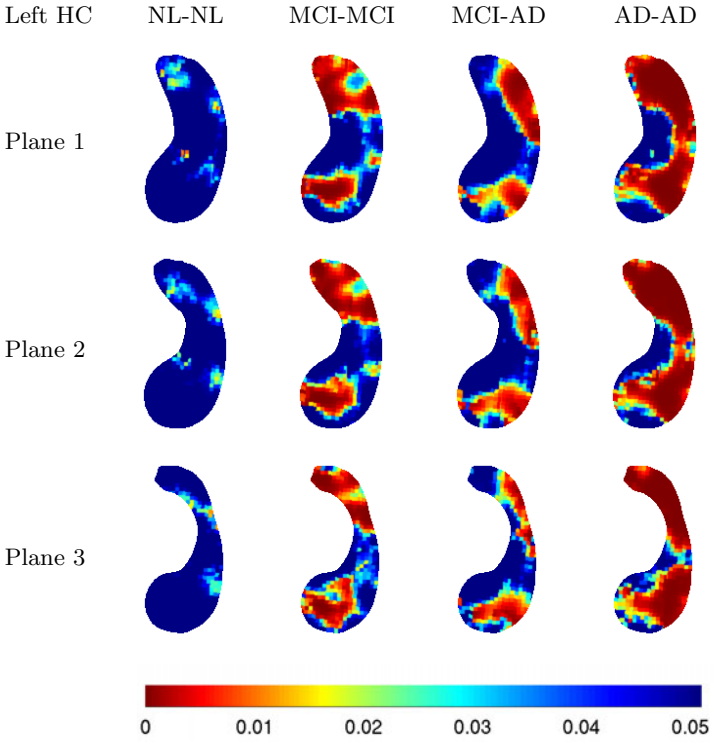

Fig. 1. Volumetric p-value maps of the comparison of the mean SEF with 0 for the left hippocampus

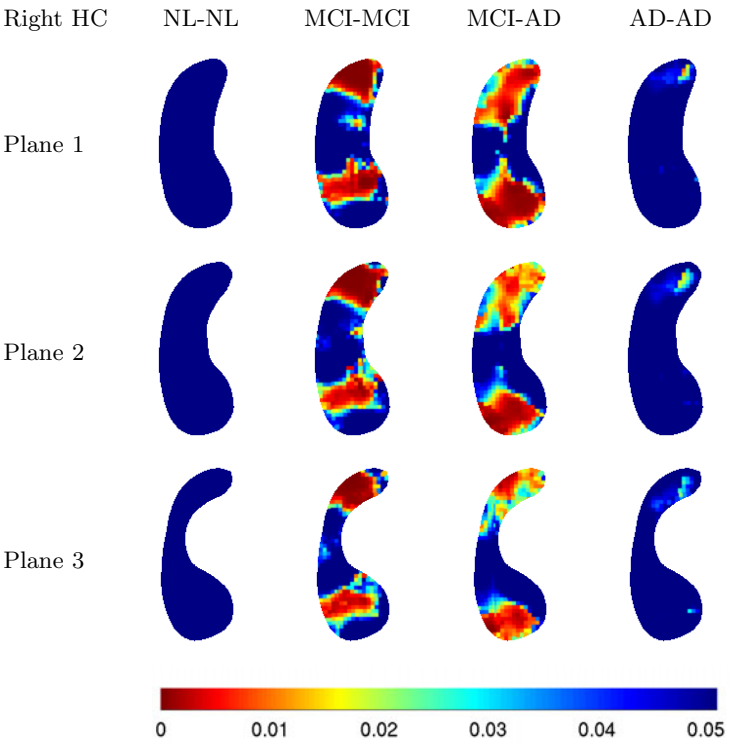

Fig. 2. Volumetric p-value maps of the comparison of the mean SEF with 0 for the right hippocampus

5.1 Correlation with Volume Loss

To simplify the computations, we focus on total volume loss and the sum of the values of each SEF over all vertices of the mesh, which we refer to as the total signed energy. The mean volume loss for the left and right hippocampi in each group is given in Table 2, where MCI-ALL is the combination of both MCI-MCI and MCI-AD. These numbers agree well with the meta-analysis of [3], which includes nine studies from seven centers, with 595 AD and 212 controls. Their study found the annualized hippocampal atrophy rates to be $4.66\%(95\%\,\mathrm{CI}\,3.92, 5.40)$ for AD and $1.41\%(0.52, 2.30)$ for controls. Another study [4] also based on the ADNI data showed a similar numerical range, with $5.59\%(95\%\,\mathrm{CI} : +/-1.44\%)$ for AD, $3.12\%(+/-0.79\%)$ for MCI and $0.66\%(+/-0.96\%)$ for controls. Two numbers in our calculations that are particularly interesting are the volume loss for the left hippocampus in the AD-AD group and the right hippocampus in the MCI-AD group, which are significantly larger than in the other groups. Table 2 also shows the mean total signed energy of each group. Again, the numbers for the left hippocampus in the AD-AD group and the right hippocampus in the MCI-AD group are relatively high.

Table 2. Mean volume loss and mean total signed energy for the left and right hippocampi in each group

Volume Loss	NL-NL	MCI-MCI	MCI-AD	MCI-ALL	AD-AD
Left HC	1.55%	2.36%	2.79%	2.44%	**5%**
Right HC	0.37%	2.76%	**4%**	3%	3.94%
Total Signed Energy	NL-NL	MCI-MCI	MCI-AD	MCI-ALL	AD-AD
Left HC	333	527	505.5	522.6	**805.9**
Right HC	116.7	508.1	**656.4**	538.2	563.7

To verify that the total signed energy correlates well with total volume loss, we calculated Pearson's linear correlation coefficients, which are shown in Table 3 and indicate that the correlation is strong. We also tested the total unsigned energy function and the correlation is much weaker and exhibit much larger variation among different groups. These results strongly support the use of SEFs for the proposed analysis of regional shape changes characteristic of tissue loss.

Table 3. Pearson's linear correlation coefficient with total volume loss

Correlation with Total Volume Loss		NL-NL	MCI-MCI	MCI-AD	AD-AD
Total Signed Energy	Left HC	0.665	0.741	0.713	0.774
	Right HC	0.742	0.78	0.794	0.793
Total Energy	Left HC	0.016	0.238	0.454	0.554
	Right HC	0.177	0.323	0.564	0.229

5.2 Group Comparison

We are primarily interested in identifying regions that exhibit morphological changes that are characteristic of local shrinkage related to tissue loss due to hippocampal degeneration over a one-year time. According to our sign convention, these regions correspond to positive values of the signed energy functions. Thus, for each of the four groups, we perform a 1-tailed t-test at each vertex to determine whether the mean SEF at that vertex is significantly larger than 0. The corresponding p-value maps for the left and right hippocampi are plotted over the hippocampal atlases and shown in Figs. 1 and 2, respectively. For visualization of these volumetric statistical maps, we sectioned the volumes along 3 planes.

As expected, the AD-AD group in Fig. 1 and MCI-AD group in Fig. 2 show larger "red" areas than the other groups. Somewhat surprising is that there is nothing significant detected for the AD-AD group in Fig. 2. This is very likely due to the high variance for this group. The average value of the variance of SEFs over all vertices is shown in Table 4. We also performed a similar experiment to analyze negative values of the signed energy functions, but nothing noteworthy was detected at comparable significance levels.

Lastly, since the left hippocampus in the AD-AD group and the right hippocampus in the MCI-AD group exhibit the most significant morphological changes, we compare them with the other groups. This time, a 1-tailed t-test at each vertex is performed to examine whether the mean of the SEFs of the

Table 4. Mean of the variance of SEFs over the vertices for the left and right hippocampi

Variance	NL-NL	MCI-MCI	MCI-AD	AD-AD
Left HC	0.39	0.59	0.42	0.72
Right HC	0.6	0.66	0.38	**1.11**

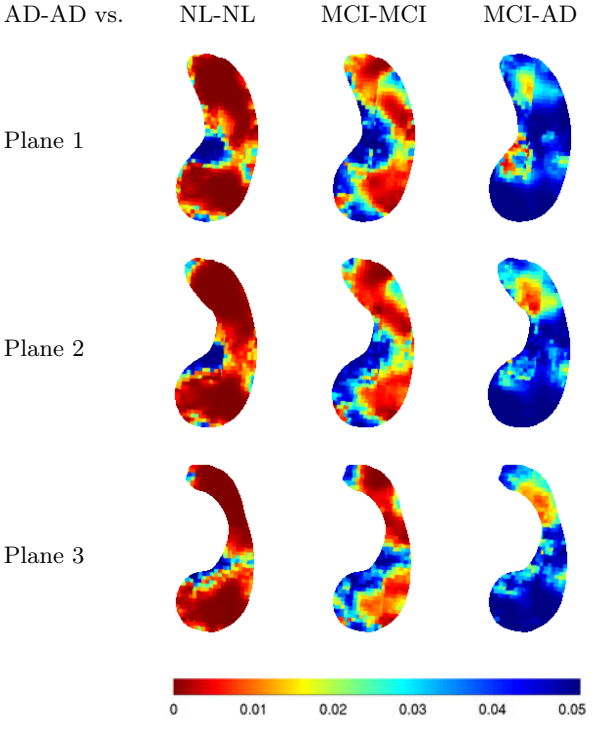

Fig. 3. Volumetric p-value maps of AD-AD versus other groups for the left hippocampus

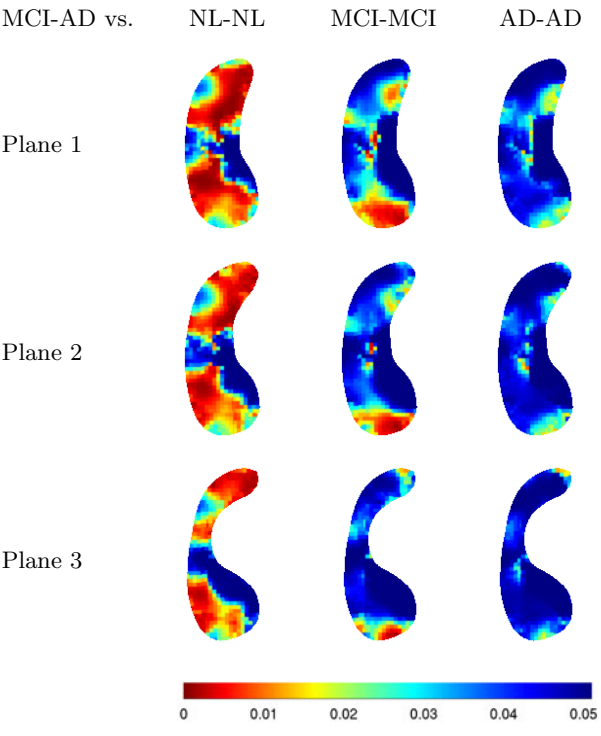

Fig. 4. Volumetric p-value maps of MCI-AD versus the other groups for the right hippocampus

reference group is significantly greater than that of the comparison group. Of course, the mean of the SEFs of the two special groups are expected to be larger. Again, the corresponding p-value maps are plotted on the hippocampal atlases in Figs. 5.2 and 4. The plot in Fig. 4 suggests that there is a specific region at the bottom of the atlas, which may be meaningful in tracking the progression of the early stage of AD, as the change of morphology in that area of the right hippocampus is highly characteristic of the conversion from MCI to AD over the one-year period.

6 Summary and Discussion

In this paper, we presented a shape model based on parametric representations of volumetric shapes. We constructed a shape space equipped with a multi-scale Sobolev-type metric, which provides a framework for the statistical analysis of shape evolution. We also introduced a signed energy function derived from the model that reflects shape changes that exhibit high correlation with regional shape shrinkage and expansion. We applied SEFs to the identification of specific

regions of the hippocampus where shape changes related to atrophy differ significantly in normal aging, conversion to Alzheimer's disease and progression of the disorder. This analysis was based on 1-year repeat magnetic resonance scans of the brain of 381 subjects collected by the Alzheimer's Disease Neuroimaging Initiative. The subjects were diagnosed as normal or with mild cognitive impairment (MCI) or Alzheimer's disease (AD) at the time of scan acquisition. Among the results obtained, we identified a region on the right hippocampus in which, according to the model, shape changes differ significantly in the MCI-AD group as compared to groups of subjects whose diagnoses did not progress beyond MCI. We also constructed p-value maps from t-tests of pointwise SEFs to visualize patterns of atrophy that differentiate the normal and pathological groups. In this work, the signs of the energy functions were chosen using a simple criterion to detect localized shrinkage, but other alternatives such as the distance to a medial curve rather the centroid of the hippocampus will be explored in future work.

References

1. Apostolova, L.G., Lu, P.H., Rogers, S., Dutton, R.A., Hayashee, K.M., Toga, A.W., Cummings, J.L., Thompson, P.M.: 3D Mapping of Mini-mental State Examination Performance in Clinical and Preclinical Alzheimer Disease. Alzheimer Disease & Associated Disorders 20, 224–231 (2006)
2. Apostolova, L.G., Dinov, I.D., Dutton, R.A., Hayashee, K.M., Toga, A.W., Cummings, J.L., Thompson, P.M.: 3D Comparison of Hippocampal Atrophy in Amnestic Mild Cognitive Impairment and Alzheimer's Disease. Brain 129, 2867–2873 (2006)
3. Barnes, J., Bartlett, J.W., van de Pol, L.A., Loy, C.T., Scahill, R.I., Frost, C., Thompson, P.M., Fox, N.C.: A Meta-Analysis of Hippocampal Atrophy Rates in Alzheimer's Disease. Neurobiol. Aging 30, 1711–1723 (2009)
4. Morra, J., Tu, Z., Apostolova, L.G., et al.: and the ADNI: Automated Mapping of Hippocampal Atrophy in 1-Year Repeat MRI Data From 490 Subjects with Alzheimer's Disease, Mild Cognitive Impairment, and Elderly Controls. NeuroImage 45(1 Suppl.), 3–15 (2009)
5. Wang, L., Beg, F., Ratnanather, T., Ceritoglu, C., Younes, L., Morris, J.C., Csernansky, J.G., Miller, M.I.: Large Deformation Diffeomorphism and Momentum Based Hippocampal Shape Discrimination in Dementia of the Alzheimer Type. IEEE Trans. Med. Imaging 26(4), 462–470 (2007)
6. Mueller, S.G., Weiner, M.W., Thal, L.J., Petersen, P.C., Jack, C., Jagust, W., Trojanowski, J.Q., Toga, A., Beckett, L.: The Alzheimer's Disease Neuroimaging Initiative. Clin. North Am. 15, 869–877, xi–xii (2005)
7. Mueller, S.G., Weiner, M.W., Thal, L.J., Petersen, P.C., Jack, C., Jagust, W., Trojanowski, J.Q., Toga, A., Beckett, L.: Ways Toward an Early Diagnosis in Alzheimer's Disease: The Alzheimer's Disease Neuroimaging Initiative (ADNI). Alzheimer's Dement. 1, 55–66 (2005)
8. Liu, X., Shi, Y., Morra, J., Liu, X., Thompson, P.M., Mio, W.: Mapping Hippocampal Atrophy with a Multi-Scale Model of Shape. In: 6th IEEE International Symposium on Biomedical Imaging, pp. 879–882. IEEE Press, Boston (2009)

9. Liu, X., Shi, Y., Wang, Y., Thompson, P.M., Mio, W.: A Riemannian Model of Regional Degeneration of the Hippocampus in Alzheimer's Disease. In: 7th IEEE International Symposium on Biomedical Imaging, IEEE Press, Rotterdam (2010)
10. Kendall, D.G.: Shape Manifolds, Prosrustean Metrics and Complex Projective Spaces. Bulletin of London Mathematics Society 16, 81–121 (1984)
11. Rosenberg, S.: The Laplacian on a Riemannian Manifold. Cambridge University Press, New York (1997)
12. Shi, Y., Thompson, P.M., de Zubicaray, G.I., Rose, S.E., Tu, Z., Dinov, I., Toga, A.W.: Direct Mapping of Hippocampal Surfaces with Intrinsic Shape Context. NeuroImage 37(3), 792–807 (2007)
13. Wahba, G.: Spline Models for Obervational Data. SIAM, Philadelphia (1990)
14. Liu, X., Mio, W., Shi, Y., Dinov, I., Liu, X., Lepore, N., Lepore, F., Fortin, M., Voss, P., Lassonde, M., Thompson, P.M.: Models of Normal Variation and Local Contrasts in Hippocampal Anatomy. In: Metaxas, D., Axel, L., Fichtinger, G., Székely, G. (eds.) MICCAI 2008, Part II. LNCS, vol. 5242, pp. 407–415. Springer, Heidelberg (2008)
15. Liu, X.: Shape Spaces, Metrics and Their Applications to Brain Anatomy. Dissertation, Florida State University (2010)